Dalton Transactions

ROYAL SOCIETY OF CHEMISTRY

FRONTIER

View Article Online
View Journal | View Issue

Cite this: *Dalton Trans.*, 2021, **50**, 4470

Efficient chemosensors for toxic pollutants based on photoluminescent Zn(II) and Cd(II) metal–organic networks

Luis D. Rosales-Vázquez, [a] Alejandro Dorazco-González *[a] and Victor Sánchez-Mendieta *[b]

Received 29th December 2020,
Accepted 1st March 2021

DOI: 10.1039/d0dt04403b

rsc.li/dalton

Optical sensors with high sensitivity and selectivity, as important analytical tools for chemical and environmental research, can be realized by straightforward synthesis of luminescent one-, two- and three-dimensional Zn(II) and Cd(II) crystalline coordination arrays (CPs and MOFs). In these materials with emission centers typically based on charge transfer and intraligand emissions, the quantitative detection of specific analytes, as pesticides or anions, is probed by monitoring real-time changes in their photoluminescence and color emission properties. Pesticides/herbicides have extensive uses in agriculture and household applications. Also, a large amount of metal salts of cyanide is widely used in several industrial processes such as mining and plastic manufacturing. Acute or chronic exposure to these compounds can produce high levels of toxicity in humans, animals and plants. Due to environmental concerns associated with the accumulation of these noxious species in food products and water supplies, there is an urgent and growing need to develop direct, fast, accurate and low-cost sensing methodologies. In this critical frontier, we discuss the effective strategies, chemical stability, luminescence properties, sensitivity and selectivity of recently developed hybrid Zn(II)/Cd(II)–organic materials with analytical applications in the direct sensing of pesticides, herbicides and cyanide ions in the aqueous phase and organic solvents.

Introduction

Coordination polymers (CPs) have attracted the attention of the scientific community for several decades.[1–3] Originally from the structural–property relationship point of view, and more recently, from the perspective of developing novel applications, CPs have risen in the past twenty-five years as one of the top functional materials to be studied, MOFs being the superstars.[4–7] The relatively easy chemical structural tuning of CPs, based on archetypal coordination chemistry, allowed the appearance, development and enhancement of their properties such as magnetism,[8] catalysis,[9] adsorption[10] and separation,[11] and luminescence;[12] it is the main reason for the increasing relevance of these interesting compounds. CPs having d-block metal ions are amongst the most prolific hybrid materials, including those containing Zn(II) and Cd(II) as metal centres, which are usually assembled using di-, tri-and tetra-carboxylate compounds or/and nitrogen compounds as bridging ligands.[13–15] These CPs are commonly exposed in a fascinating structural diversity due to their inherent metal-linker joining in the current and on-going, well-documented, secondary building units (SBUs).[16,17] Regardless of the substantial number of Zn and Cd based coordination frameworks structurally characterized, thorough studies in relation to their fluorescence properties, and their use as chemosensors for diverse analytes, remain an open challenge.[18,19] Hence, growing interest in their applications towards the recognition and detection of environmental hazardous species has been reflected in freshly day-to-day emerging literature and, consequently, in cutting-edge and excellent reviews.[4,19–21] Special attention in this line has been focused on toxic compounds, such as energetic materials (explosives), cations and anions.[4,19,20] Even though the detection of those compounds is important and, therefore, further studies should continue, in the last years there has been a bullish awareness for the sensing of pesticides and herbicides, which, at some level, had been an overshadowed issue in detection studies of hazardous pollutants by luminescent CPs and MOFs. Taking into consideration the crucial role that farming activities play in our lives, at least one-third of the global agricultural production is highly dependent on pesticides and herbicides.[22] Some of the biggest problems of these anthropogenic pollutants are their high tox-

[a]*Instituto de Química, Universidad Nacional Autónoma de México. Circuito Exterior, Ciudad Universitaria, Ciudad de Mexico, 04510, Mexico. E-mail: adg@unam.mx*
[b]*Centro Conjunto de Investigación en Química Sustentable UAEM-UNAM, Carretera Toluca-Ixtlahuaca Km. 14.5, San Cayetano, Toluca, Estado de Mexico, 50200, Mexico. E-mail: vsanchezm@uaemex.mx*

icity, along with their poor selectivity to differentiate between target and non-target populations. This indiscriminate usage has been exposed in studies where only 1% (sometimes even lower[23]) of the sprayed pesticides actually reaches the targeted species. The remaining 99% of the applied pesticides tends to bio-accumulate in the food chain and drift in the environment *via* rivers, lakes or other bodies of water causing irreparable damage to the flora and fauna, and also to humans in the form of numerous health-related issues.[22–26] Although some political measures have been addressed in order to reduce the negative impact of pesticides and herbicides (programs like ECOPHYTO by the French government),[23] there is still a long road ahead to lessen this trouble. In addition, to the best of our knowledge, the extremely lethal cyanide ion represents another example of an overlooked toxic pollutant not often mentioned in the up-to-date literature of luminescent CPs.[20,27,28] Despite its inherent danger, curiously, the cyanide ion is repeatedly ignored in the research of anionic contaminants detected using coordination frameworks.[4,15,19,27–29] Bearing this in mind, we decided to integrate this interesting yet dangerous anion to the discussion in order to raise awareness for further related investigations.

This Frontier article highlights selected examples and current advances in the effectiveness of luminescent Zn and Cd CPs and MOFs as highly sensitive, selective, and relatively low-cost fluorescent sensors for the real-time detection of pesticides, herbicides and the cyanide ion, believing that these versatile hybrid materials would eventually contribute to the monitoring and control of the excessive use of hazardous pollutants, minimizing their effects on the environment.

General design outline of luminescent Zn(II)/Cd(II) coordination polymers for pesticide/herbicide sensing

From a synthetic point of view, the straightforward combination of d^{10} metal centers (Zn(II) or Cd(II)) and appropriate organic polytopic linkers, such as aromatic multicarboxylates or N-donor ligands, can be used to obtain CPs with appealing structural diversity,[30] exhibiting a large number of photoluminescence processes.[12,19,31–33]

The effective interaction between diamagnetic d^{10} transition-metal centers and this type of ligand enhances the fluorescence emission due to the increase of the rigidity of the aromatic ligand inside the final crystal arrangement, which reduces the loss of energy through non-radiative processes.[31,34]

The rational design of efficient Zn(II)/Cd(II) CPs for luminescence sensing of pesticides and anions must include materials with the following features: (1) chemical stability, specifically under the desired sensing conditions (aqueous media, physiological environments, real samples with multiple interferents), (2) a stable luminescence source, and (3) specific sites of recognition for the target analyte capable of generating a selective optical response (Scheme 1).

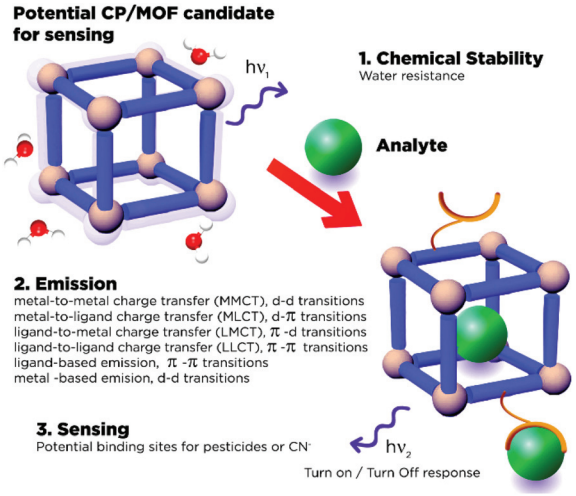

Scheme 1 Schematic overview of the design of a potential transition-metal CP/MOF for real world sensing applications considering the importance of chemical stability in water and specific binding sites.

Chemical stability of Zn(II)/Cd(II) CPs and MOFs in water

Luminescent Zn(II)/Cd(II) CPs and MOFs have been widely used as chemosensors for direct optical detection of anions (halides, pseudohalides and carboxylates),[35–37] transition-metal ions (Cu(II), Zn(II), Hg(II) Cr(III), Cr(VI), Fe(III)),[29,34,38–42] amino acids (*e.g.*, histidine and aspartic acid),[28,43] nitroaromatic explosives,[44–47] volatile organic compounds (VOCs),[48–50] organoamines,[51] and pollutant gases,[27] as pH-sensors,[35] and in lesser use for antibiotics[52–55] and biomarkers of carcinoid tumors.[56]

Although the literature shows very recent examples (made post 2014) of sensors based on Zn(II)/Cd(II) CPs for pesticides (Schemes 2–4) such as parathion,[23,57,58] paraoxon,[57] fenitrothion,[57] glyphosate,[25] azinphos-methyl,[59,60] chlorpyrifos,[61] 2,6-dichloro-4-nitroaniline, (DCN);[24,29,37,62,63] trifluralin, (TFL);[24] nitenpyran,[64] simazine,[65,66] 2,4,6-trichloroanisole, (TCA);[65] diquat, (DQ);[67] and paraquat (PQ),[68] some analytical aspects such as selectivity, efficient optical response, functionality in complex or real samples, and chemical stability in aqueous media persist as central drawbacks in these reported systems.

On the other hand, cyanide sensing by luminescent Zn(II)/Cd(II) CPs in pure water still remains largely unexplored, despite the fact that the examples reported in the literature (only three studies) show efficient analytical responses with very low detection limits ($<10^{-6}$ M), selectivity over common interfering anions and structural advantages compared to conventional organic luminophores.[69–71] In general, the development of d^{10} metal CP/MOF-based sensors has been largely restricted to non-aqueous media which seriously limits their applications.[24,57,62,65,66,72,73]

The chemical stability of CPs and MOFs in the presence of water is a critical property and prerequisite when considering

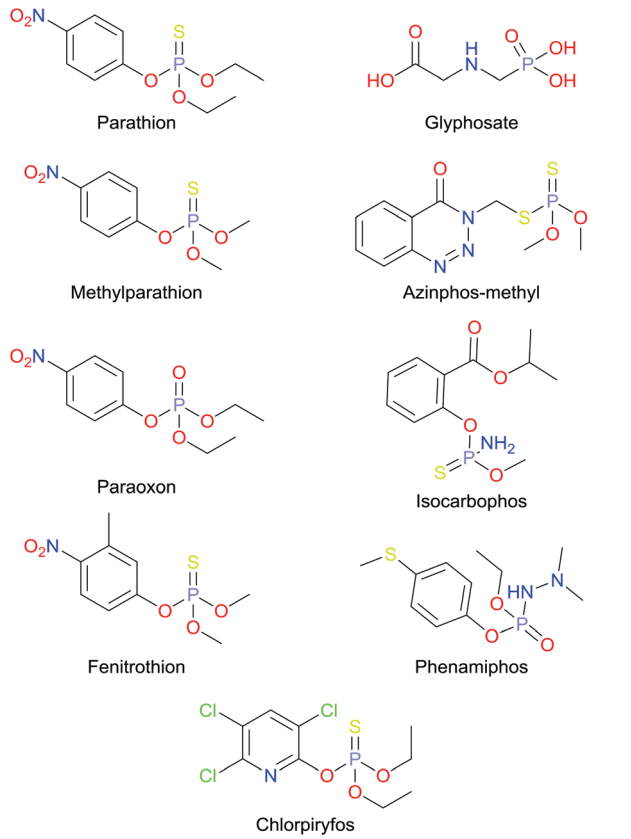

Scheme 2 Chemical structures of the main organophosphate pesticides.

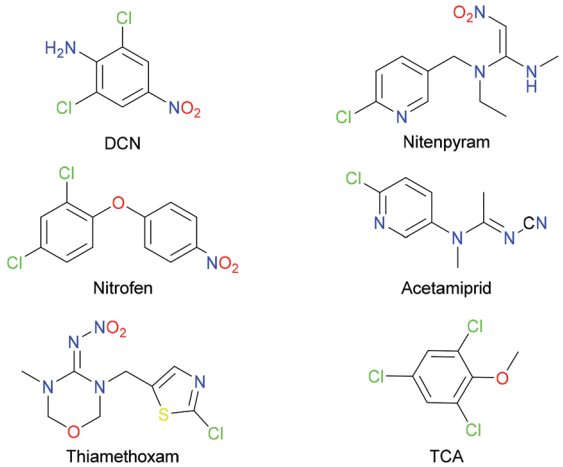

Scheme 3 Chemical structures of the main organochlorine pesticides.

these materials for luminescence sensing applications in real-world samples.

A hydrostable CP/MOF is a material that can be handled in aqueous solutions and is expected to maintain its chemical structure. Experimentally, this stability can be inferred through exposure of the sample (CP) to aqueous conditions and subsequent comparison of the sample's structural properties before and after water exposure *via* methods such as fluorescence spectroscopy, IR-spectroscopy and powder X-ray diffraction.[74] For luminescent CPs/MOFs, the simplest and most common method to study the chemical stability in aqueous media is to record the emission spectra of aqueous suspensions or solutions as a function of time and to compare them with the initial spectrum of the starting material.[71] This method works well as a first-pass evaluation of hydrolytic stability, but a sample with small changes in its emission intensity, even without displacements of its emission maxima, can undergo changes in its chemical structure, for example, a dynamic solvent exchange by water molecules.[75]

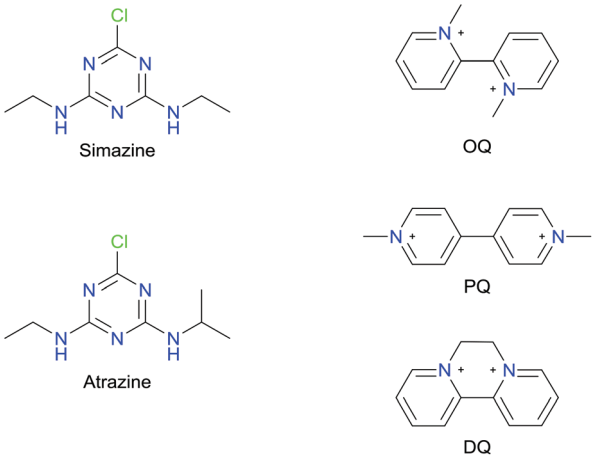

Scheme 4 Chemical structures of the main herbicides.

In thermodynamic terms, hydrostable CPs include a combination of inert metal nodes (mononuclear or cluster) and ligands which makes energetically unfavourable the irreversible hydrolysis reaction (1).

$$\Delta G_{\mathrm{hyd}} = \Delta G_{\mathrm{prod}}(\mathrm{CP} + n\mathrm{H_2O}) + \Delta G_{\mathrm{react}}\ (\mathrm{CP} + n\mathrm{H_2O}) \qquad (1)$$

where ΔG_{prod} is the free energy of the aqua coordination polymer formed between the CP and the water molecules after the hydrolysis reaction takes place and $\Delta G_{\mathrm{react}}$ is the free energy of the CP and the water molecules before the hydrolysis occurs.

In these materials, the strength of metal–ligand coordination bonds can be a strong indicator of their hydrolytic stability. As a weak point in these synthetic structures, usually, the metal–ligand bond strength is less compared to that of natural hydrostable materials such as zeolites. In principle, the hydrolytic stability of these CPS and MOFs requires sufficient metal–ligand binding free energy to overcome the high hydration energies of Zn(II)/Cd(II) ions (ΔG = −2043 and −1843 kJ mol^{-1} for Zn(II) and Cd(II), respectively).[76]

Because Zn(II)/Cd(II) CPs are governed by Lewis acid–base coordination chemistry, the pK_a of the coordinating atom on the ligand can be used as a first approximation of the metal–ligand bond strength. This correlation was previously

studied by Long and used as a strategy for the preparation of a series of highly hydrostable Co(II), Zn(II), Ni(II), and Cu(II) based MOFs containing the pyrazolate ligand.[77]

As the hydrolysis reaction of Zn(II)/Cd(II)-based CPs can only proceed if the water molecule comes sufficiently close to the metal to allow the interaction between the electron orbitals on the electrophilic metal and nucleophilic water molecule, the introduction of hydrophobic fragments in the ligands is a common approach to improve the hydrostability and decrease the degree of hydration of the metallic nodes without compromising the chemical structure of Zn(II)/Cd(II)-CP based sensors.[50,74]

Luminescence of Zn(II)/Cd(II) CPs and MOFs

The luminescence of Zn(II)/Cd(II)-CPs containing aromatic multicarboxylates or N-donor ligands stems from several processes such as ligand-centered emission (LC), metal-centered emission (MC), ligand-to-metal charge transfer (LMCT), metal-to-ligand charge transfer (MLCT) and ligand-to-ligand charge transfer (LLCT) and even analyte-induced luminescence as depicted in Scheme 1. Among these kinds of emissions, the most commonly reported ones for CPs and MOFs containing Zn(II)/Cd(II) are LC, LLCT and LMCT, the latter is observed especially when CPs and MOFs have Zn(II)/Cd(II) clusters as nodes.[19,78]

In this context, organic carboxylate ligands included in the most common CPs and MOFs contain π-conjugated backbones which have little spin–orbit coupling, so the emission is determined basically by the excited states of the ligand with the electronic transition π–π* or n–π* and the symmetry of the singlet ground state.[79] Thus, the emission is typically from the lowest excited singlet state to the singlet ground state (fluorescence). LMCT-based emission has been reported in a wide range of Zn(II) and Cd(II) CPs/MOFs, which involve electronic transitions from an organic linker localized orbital to a metal-centred orbital; this mechanism occurs primarily in structures containing benzene-multicarboxylates as linkers and N-donors as auxiliary ligands.[79] Usually, these materials display intense blue and green emissions in the range of 380 nm–500 nm.[79–81] For recent examples see: $[Cd_{1.5}(dpb)(2,2'\text{-bpy})]$,[32] [Zn(dbpy)(DMF)],[44] $[Cd(tptc)_{0.5}(2,2'\text{-bipy})]$,[82] $[Cd_3(dtba)_3(bbp)_3]$[83] and $[Cd_3(tma)_2(iQ)_3(DMF)]$[84] (Hdpb = 3-(2′,3′-dicarboxylphenoxy)-benzoic acid; H_2dbpy = 2,2′-bipyridine-4,4′-dicarboxylate, H_4tptc=(1,1′:4′,1″-terphenyl)-2′,3,3″,5′-tetracarboxylic acid, H_2dtba = 2,2′-dithiobisbenzoic acid, bpp = 1,3-bis(4-pyridyl)-propane, H_3tma = trimesic acid and iQ = isoquinoline), where the trinuclear Cd-MOFs display room temperature blue luminescence at ∼435 nm with a lifetime in the nanosecond range attributed to a combination of intraligand emission and LMCT. Generally, these types of metal–organic networks containing Zn(II)/Cd(II) ions with benzene-multicarboxylate and aromatic N-donors exhibit enhanced blue emission peaks at 400–500 nm in comparison to free ligands, which can be attributed primarily to a combination of metal perturbed intra-ligand emissions (LC and LLCT) and LMCT.[5,24,29,37,47,57,58,79,86]

The possible electronic states involved in the luminescence phenomenon of Zn(II)/Cd(II)-based MOFs are listed in Scheme 1. To understand the nature and general aspects of this luminescence concept, the readers should refer to specific reviews on the subject.[12,78,81]

Frequent photophysical approaches, based on luminescence signal changes, for the detection of heavy-atom anions, cyanide ions and pesticides in Zn/Cd metal–organic networks, include (1) photoinduced electron transfer (PET),[5,24,37,62,67,68,86,103] (2) Förster resonance energy transfer (FRET)[5,19,27,36,52,63,79] and (3) charge transfer.[79]

For toxic pollutant and cyanide sensing, the PET mechanism is the most popular, and has been used to develop many "turn-off" fluorescent chemosensors.[5,24,37,62,67,68,86,103] PET-based electron donor–acceptor metal–organic networks can be understood in the light of frontier molecular orbital theory. In the presence of the analyte, the HOMO of the donor (anion or analyte) lies higher in energy than the acceptor (luminescent chemosensor), which results in an electron transfer to the acceptor's HOMO immediately after excitation and before emission, thereby quenching luminescence.[5]

Selectivity towards pesticides/herbicides

The use of commercial pesticides with life-threatening health effects (*e.g.*, neurotoxicity, genotoxicity and cancer)[85] and serious adverse environmental impacts[22] forces the development of efficient real-time quantification sensing systems, with high sensitivity and selectivity. While the need for efficient and highly selective optical chemosensors for pesticides is evident, to date, very few sensory systems capable of operating in 100% water and real samples have been described, which is highly desirable for practical application.

For CPs/MOFs with one type of emission source, the change in the monochromatic luminescence signal in the presence of a pesticide is good and enough for the quantitative analysis; however, the selectivity is still not comparable to those of HPLC techniques and mass spectrometry (GC-MS); furthermore, most reports lack studies on complex or real samples (Table 1).

In contrast, remarkable progress in the development of systems with very high sensitivity and low detection limits, in the nanomolar range ($<10^{-7}$ M), for several pesticides has been achieved using high-dimensional porous d^{10}-based MOFs such as $[Zn_4(TCPP)_2(TCPB)_2]$,[23] $[Cd_3(PDA)(tz)_3Cl(H_2O)_4]$,[59] $[Cd_2(tib)(btb)(H_2O)_2]$,[64] and ZnPO-MOF[86] and Zn(II)-coordination polymers such as Zn-NDC-MI[63] (see Table 1 for abbreviations).

Owing to the toxicity of these pollutants, the World Health Organization (WHO) is under a strong vigilance of their permissible limits in drinkable water (glyphosate: 4.14×10^{-6} M; chlorpyrifos: 8.57×10^{-8} M; trifluralin 5.96×10^{-8} M; simazine 1.98×10^{-8} M; atrazine 1.39×10^{-8} M and DQ 1.08×10^{-7} M), keeping also close monitoring of several other pesticides and herbicides in accord to their impact on human health.[94] Additionally, the Food and Agriculture Organization (FAO) from the United Nations has also established rigorous maximum residue limits (MRL) for each pesticide and herbicide varying according to the type of fruit, vegetable or seed.[95]

Table 1 Comparison of the structural characteristics and analytical parameters of selected chemosensors for toxic pollutants

Sensor	Compound	Structural dimensionality	Synthesis method	Fluorescence response	Target analyte	System	λ_{em}	Sensitivity (LOD) M	Ref./ year
1	MOF-5	3D	Room temperature	Turn-off	Parathion, methyl-parathion, paraoxon, fenilthion	EtOH	493	10^{-5}	57
2	NMOF1 ([Cd(atc)(H_2O)$_2$]n, antíparathion complex	3D	Room temperature	Turn-off	Parathion	H_2O	424	3.43×10^{-6}	58
3	[Zn_4(TCPP)$_2$(TCPB)$_2$]n	[a]	Solvothermal	Turn-off	Parathion	H_2O (real irrigation sample)	380	6.69×10^{-9}	23
4	[Zn(pbdc)(bimb)·(H_2O)]n	3D	Solvothermal	Turn-off	Methylparathion	DMF	355	2.5×10^{-6}	72
5	ZnPO-MOF	3D Micropore structure	Solvothermal	Turn-off	Methylparathion	EtOH–H_2O (real irrigation sample)	≈410[a]	4.56×10^{-10}	86
6	[Cd_8(D-cam)$_8$(bimb)$_4$]n	2D	Solvothermal	Turn-off	Methylparathion	DMF	370	3.6×10^{-6}	73
7	MOF-Calix	2D Nanosheets	Solvothermal	Turn-on	Glyphosate	MeOH–isopropanol–H_2O	329	2.25×10^{-6}	25
8	[$Cd_{2.5}$(PDA)(tz)$_3$]n	3D	Solvothermal	Turn-off	Azinphos-methyl	H_2O (extract from apples)	290	5×10^{-5}	60
9	[Cd_3(PDA) (tz)$_3$Cl(H_2O)$_4$]·3H_2O	3D	Room temperature	Turn-off	Azinphos-methyl	H_2O (extract from apples and tomatos)	290	2.5×10^{-8}	59
10	{[Zn_3(Hdpa)(OH) (H_2O)$_2$]·6H_2O}n	3D	Solvothermal	Turn-off	Chlorpyrifos	H_2O	350	[a]	61
11	[Cd_2((1*R*,2*R*/1*S*,2*S*)-Hcpba)$_2$(phen)$_2$]n	1D	Solvothermal	Turn-off	DCN	DMF	≈420[a]	1.12×10^{-6}	62
12	(H_3O)[Zn_2L(H_2O)]·3NMP·6H_2O	3D	Solvothermal	Turn-off	DCN, TFL	NMP	440	1.41×10^{-5}	24
13	[Zn_3(DDB)(DPE)]·H_2O	3D	Solvothermal	Turn-off	DCN	H_2O (extract from carrots, nectarines and grapes)	≈450[a]	2.7×10^{-7}	37
14	[Zn_2(L^2)$_2$(TPA)]·2H_2O	2D	Solvothermal	Turn-off	DCN	MeOH	432	1.9×10^{-3}	29
15	{[Zn(L^3)(1,4-bdc)$_2$·2(1,4-H_2bdc)]}n	3D	Solvothermal	Turn-off	DCN	H_2O	≈375[a]	1.29×10^{-3}	96
16	Zn-NDC-MI	2D	Solvothermal	Turn-off	DCN	H_2O	369	6×10^{-8}	63
17	[Cd_2(HDDB)(bimpy)(NMP) (H_2O)]·3H_2O	2D	Solvothermal	Turn-off	DCN	H_2O	462	3.6×10^{-7}	97
18	{[Cd(tptc)$_{0.5}$(bpz)(H_2O)]·0.5H_2O}n	2D	Solvothermal	Turn-off	DCN	H_2O	392	5.4×10^{-7}	98
19	[Cd (tptc)$_{0.5}$(bpy)]n	2D	Solvothermal	Turn-off	DCN	H_2O	392	3.08×10^{-6}	98
20	NUC-6	3D	Solvothermal	Turn-off	DCN	H_2O	392	5.6×10^{-7}	99
21	[Zn_2(bpdc)$_2$(BPyTPE)]	3D	Solvothermal	Turn-off	DCN	DCM	498	6.27×10^{-7}	100
22	[Cd_3(CBCD)$_2$(DMAc)$_4$ (H_2O)$_2$]·10DMAc	3D	Solvothermal	Turn-off	DCN	DMAc	≈430[a]	7×10^{-7}	101
23	Rho B@ [Cd_2(tib)(btb)(H_2O)$_2$]·NO_3·2DMF	3D	Solvothermal	Turn-off	Nitenpyram	H_2O, DMF	590, 606	4.8×10^{-10}	64
24	Rho 6G@ [Cd_2(tib)(btb) (H_2O)$_2$]·NO_3·2DMF	3D	Solvothermal	Turn-off	Nitenpyram	H_2O, DMF	590	3×10^{-9}	64
25	{[Cd(μ_2-BA)$_2$(ClO_4)$_2$]·n(DCM)}n	2D	Room temperature	Turn-off	Simazine, TCA	MeCN	450	4.78×10^{-7}	65
26	Cd·AHP·2,6-NDS·DMF·2H_2O	2D	Solvothermal	Turn-off	Simazine	DMF	≈440[a]	2.25×10^{-4}	66
27	[$Zn_{1.5}$(DBC)·(H_2O)·(DMF)·Me_2NH_2]n	3D	Solvothermal	Turn-off	DQ	H_2O	420	1.52×10^{-5}	67
28	[Zn_2(cptpy)(btc)(H_2O)]n	3D	Solvothermal	Turn-off	PQ	H_2O	400	9.73×10^{-6}	68
29	{[Zn_2(H_2O)$_2$(*e*,*a*-cis-1,4-chdc)$_2$(4,4′-dtbb)$_2$]·7H_2O}n	1D	Room temperature	Turn-off	CN^-	H_2O	434	9×10^{-8}	71
30	M-ZIF-90	3D	Solvothermal	Turn-off	CN^-	H_2O–DMSO	450	2×10^{-6}	69
31	Bio-MOF-1 ⊃ DAAC	3D	Solvothermal	Turn-on	CN^-	H_2O	510	1.9×10^{-8}	70

Abbreviations: [a] = Not specified, atc = aminoterephthalic acid, TCPP = tetrakis (4-carboxyphenyl)porphyrin, TCPB = 1,2,4,5-tetrakis (4-carboxyphenyl)benzene, pbdc = 5-(4-pyridyl)-isophthalic acid, bimb = 4,4′-bis(1-imidazolyl)biphenyl), ZnPO-MOF = [Zn_2(Zn-(5,15-dipyridyl-10,20-bis(pentafluorophenyl))porphyrin)(1,2,4,5-tetrakis(4-carboxyphenyl)benzene)]n, D-cam = D-camphor acid, Calix-MOF = {[Cd_2(5-NO_2-BDC)$_2$$L^4$(MeOH)]$_2$·MeOH}$n$ L^4 = 25,26,27,28-tetra-[(4-pyridylmethyl)oxy]calix[4]arene, PDA = 1,4-phenylenediacetate, tz = 1,2,4-triazolate, (1*R*,2*R*/1*S*,2*S*)-H_3cpba = (1*R*,2*R*/1*S*,2*S*)-2,2′-((5-carboxy-1,3-phenylene)bis(oxy))dipropionic acid, phen = 1,10-phenanthroline, L = 2,5-(6-(4-carboxyphenylamino)-1,3,5-triazine-2,4-diyldiimino, BPyTPE = (*E*)-1,2-diphenyl- 1,2-bis(4-(pyridin-4-yl)phenyl)ethane, DDB = 3,5-di(2′,4′-dicarboxylphenyl)benzoic acid, DPE = 1,2-di(4-pyridyl)ethylene, L^2 = 4-(tetrazol- 5-yl)phenyl-4,2′:6′,4″-terpyridine, TPA = terephthalic acid, L^3 = bis(4-(4*H*-1,2,4-triazol-4-yl)phenyl)methane, bdc = 1,4-benzenedicarboxylic acid, NDC = 2,6-naphthalenedi-carboxylate, MI = 2-methylimidazole, CBCD = 4,4′-(9-(4′-carboxy-[1,1′-biphenyl]-4-yl)-9*H*-carbazole-3,6-diyl)dibenzoic acid, DMAc = *N*,*N*-dimethylacetamide, Rho = Rhodamine, btb = 1,3,5-benzenetribenzoic acid, tib = 1,3,5-tri(1-imidazolyl)benzene, H_6dpa = 3,4-di(3,5-dicarboxyphenyl)phthalic acid, NMP = *N*-methylpyrrolidone, tptc = *p*-terphenyl-2,2″,5″,5‴-tetracarboxylate acid, bpz = 2-(1*H*-pyrazol-3-yl)pyridine, bpy = 2,2′-bipyridine, bpdc = biphenyl-4,4′-dicarboxylic acid, BPyTPE = (*E*)-1,2-diphenyl-1,2-bis(4-(pyridin-4-yl)phenyl)ethene), BA = bis-9,10-(pyridine-4-yl)-anthracene, DMF = *N*,*N*-dimethylformamide, AHP = 1,1′-(anthracene-9,10-diylbisIJmethylene))bisIJpyridin-1-ium-4-olate), 1,5-NDS = 1,5- naphthalenedisulfonic acid, SIA = 5-sulfoisophthalic acid, DBC = 2,7,10,15-tetrakis[2,6-dimethyl-4-(α-carboxy)methoxyphenyl]-dibenzo[*g*,*p*]chrysene, cptpy = 4-(4-carboxyphenyl)-2,2′:4′,4″-terpyridine, btc = 1,3,5-benzenetricarboxylic acid, 1,4-chdc = 1,4-cyclohexanedicarboxylato, 4,4′-dtbb = 4,4′-di-*tert*-butyl-2,2′-bipyridine, DAAC = 3,6-diaminoacridinium cation DCN = 2,6-dichloro-4-nitroaniline, ZIF = zeolitic imidazolate framework DQ = diquat, PQ = paraquat, TCA = 2,4,6-trichloroanisole, and TFL = trifluralin.

In this context, luminescent Zn(II) and Cd(II) crystalline metal–organic networks have gained extensive attention as optical sensors for pesticides because of their straightforward synthesis, fast response, high selectivity and sensitivity, and recyclability. A notable example is the 2D nano-sheets of MOF-Calix[25] (Table 1) which showed excellent sensing performance of glyphosate, which is the most frequently used herbicide worldwide, with a low limit of detection of 2.25×10^{-6} M with a luminescence "turn-on" response. This limit of detection is below the maximum permissible limit of the WHO in drinking water (4.1×10^{-6} M).[25,94]

Although great advances have been made in the development of chemosensors based on metal–organic materials for the detection of pesticides, most reports lack studies on complex or real samples. Some notable examples are the compounds $[Zn_4(TCPP)_2(TCPB)_2]n$[23] and ZnPO-MOF,[86] which were used in the determination of parathion and methyl-parathion directly in irrigation water with detection limits in the nanomolar concentration range (Table 1) with excellent recovery rates. These detection values are much lower than the maximum residual limits in the European Pesticides databases (*e.g.*, 1.7×10^{-6} M for parathion)[23]

On the other hand, the literature shows a very few examples of these types of chemosensors for pesticides in fruits and vegetables. Water-stable trinuclear MOFs $[Cd_3(PDA)(tz)_3Cl(H_2O)_4]\cdot 3H_2O$[59] and $[Zn_3(DDB)(DPE)]\cdot H_2O$[37] (Table 1) are able to detect azinphos-methyl and 2,6-dichloro-4-nitroaniline (DCN), respectively, in apples, fruit extracts and tomatoes with the detection limit in the nanomolar concentration range. These detection limits meet the maximum residue limits established by the Food and Agriculture Organization (FAO) of the United Nations (*e.g.*, MRL = 3.15×10^{-6} M for azinphos-methyl in tomatoes).[37,59]

CP/MOF-based sensors have immense possibilities for the functionalization of specific binding sites, the activation of pendant groups, pore size modulation, suitable signal transduction and post-synthetic modification.[22] Despite the significant advances that have been made in luminescence sensing systems for pesticides, the selectivity is a current unsolved challenge.[22]

Regarding biological receptors, the substrate molecules selectively bind to a specific site typically with multiple converged and complementary host–guest interactions.[87] To date, the pore size modulation of MOFs and the electron-donating property modulation of the ligands have been an important strategy to provide close interactions between the metal–organic frameworks and analytes (pesticides), thus generating selective systems. Some notable examples are Zn(II)-MOFs $[Zn_4(TCPP)_2(TCPB)_2]n$ and ZnPO-MOF where the selectivity towards parathion and methyl parathion over several organophosphate derivatives is attributed to the strong electron transfer from the electron-donating ligands to the highly electron-withdrawing nitroaromatic group in the pesticides.[23,86] These materials were used in the determination of methyl parathion in irrigation water with satisfactory results.

Previously mentioned MOF-Calix is a selective sensor designed with the concept of host–guest chemistry, where the MOF binds to glyphosate by multiple hydrogen bonding and π···π stacking interactions.[25] The selectivity of the three-dimensional MOF $[Cd_3(PDA)(tz)_3Cl(H_2O)_4]\cdot 3H_2O$ is attributed by the authors to the integration of various convergent interactions such as hydrogen bonding and π···π stacking between the MOF and the pesticides, whilst the selectivity of $[Cd_{2.5}(PDA)(tz)_3]n$ is the result of the combination of π···π interactions between the aromatic part of azinphos-methyl and the aromatic panel of the MOF together with a strong coordination bond (Cd···S=P) between the terminal S atom of azinphos-methyl and the Cd(II) atom.

Selectivity towards cyanide

Nowadays, a large amount of metal salts of cyanide is widely used in several industrial processes (~1 400 000 tons per year)[88] such as gold mining, and plastic manufacturing.[89] Cyanide waste causes serious pollution in the environment, especially in natural water sources. Compared with very toxic heavy-metal ions, CN^- can lead to the death of humans and aquatic species in minutes.[90] For this reason, the development of sensitive and selective CN^- sensors capable of operating in the aqueous phase has been a subject of intense research during the last few decades.[91]

The literature shows very few examples of cyanide sensing by metal–organic materials.[69–71] Ghost and coworkers reported the first two examples of post-synthetically modified MOF-based chemical sensors for CN^- in the aqueous phase.[69,70] Post-synthetic modification was employed to incorporate a specific recognition site for CN^- (reactive free aldehyde groups aligned within the pores) with selectivity over halides, oxoanions and pseudohalides.

Recently, Sánchez-Mendieta and co-workers reported a series of hydrolytically stable zinc-1,4-cyclohexanedicarboxylato coordination polymers, with blue emission, capable of selectively quantifying cyanide ions with a detection limit of 9×10^{-8} M.[71] The selectivity was attributed by the authors to the coordination of the cyanide anion with the metallic centre, which resulted in the formation of the salt $Zn(CN)_2$ with the simultaneous release of the ligands. The nucleophilicity of the cyanide anion together with the high hydration energies of other anions such as halides and oxoanions makes these polymers efficient to function as cyanide-selective fluorescent chemodosimeters over a wide pH range.

Interestingly, Zn(II)-metal–organic materials designed for cyanide sensing have detection limits (~ 10^{-8} M) considerably lower than the maximum level of CN^- recommended by the WHO in drinking water (2.7×10^{-6} M).[69–71]

CPs and MOFs as fluorescent sensors of pesticides

In one of the earliest instances, the well-known MOF-5 has been applied by Kumar's group in the luminescence detection

of organophosphate pesticides (OPPs) such as parathion, methylparathion, paroxon (an initial degradation product of parathion) and fenitrothion (Scheme 2).[57]

Usually, most of the OPPs are potent nerve agents that can irreversibly inhibit the activity of the acetylcholinesterase enzyme (AChE), which is responsible for the proper functioning of the nervous system by hydrolysing the neurotransmitter acetylcholine (ACh). Since ACh is an important neurotransmitter, the over-accumulation of ACh eventually leads to respiratory paralysis and death.[23,59] Although no selectivity over any of the OPPs mentioned was shown for MOF-5, Kumar's group continued their investigations into the recognition of OPPs with NMOF1, a cadmium and 2-aminoterephthalic acid based 3D MOF, with the particular characteristic of a non-coordinative –COOH group, which was post-synthetically converted into an amide by the reaction with EDC (1-ethyl-3-(3-dimethyl aminopropyl) carbodiimide), enhancing in the MOF the capacity of bioconjugation with a selective antibody against parathion (NMOF1/anti-parathion) (Fig. 1). The sensitivity of the system was increased up to 5-fold in comparison to that of MOF-5 and the analysis was proceeded in an aqueous medium with a quenching response.[58]

Likewise, the fluorescence recognition of methylparathion has been achieved using ZnPO-MOF, a 3D microporous MOF constituted of a metalloporphyrin (Zn-(5,15-dipyridyl-10,20-bis(pentafluorophenyl))porphyrin) and a tetracaboxylate linker (1,2,4,5-tetrakis(4-carboxyphenyl)benzene) assembled together through the typical Zn-paddlewheel SBU.[86] The MOF experienced a significant change in its fluorescence signals with a selective turn-off response for methyl-parathion, which was attributed to the PET mechanism.[86] Importantly, methyl-parathion detection can be carried out in competition with several OPPs and other nitroaromatic compounds, and it has confirmed its efficacy in real irrigation samples from a lake.[86]

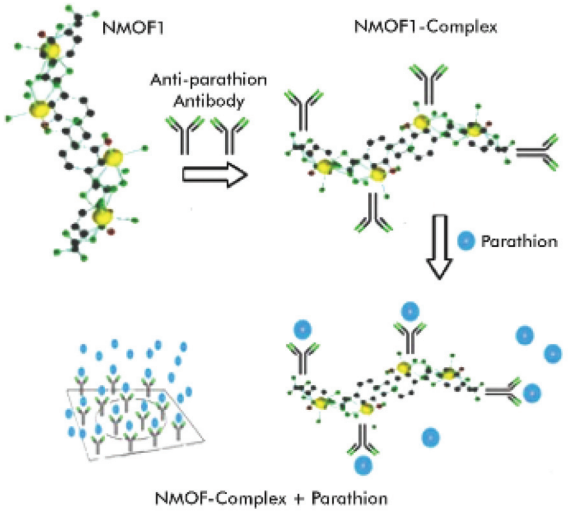

Fig. 1 Mechanism for parathion detection using NMOF1. Modified with permission from ref. 58 copyright (2020) Elsevier.

Furthermore, in an on-going process, glyphosate, the active ingredient in most Roundup® brand pesticides and other weed-control products of the same producing company, has been in the spotlight for recent carcinogenic allegations. With the growing importance of the rapid detection of glyphosate, Yu's group has designed a specific glyphosate fluorescent sensor.[25] Their synthetic strategy relies on the incorporation of a predesigned tetra-pyridyl-functionalized calix[4]arene ligand (25,26,27,28-tetra-[(4-pyridylmethyl)oxy]calix[4]arene) which reacted with 5-nitro-1,3-benzenedicarboxylic acid (5-NO_2-BDC) and $Cd(NO_3)2{\cdot}4H_2O$, producing a 2D functionalized cup-shaped feature structure attributable to the calix[4]arene ligands, where those layers are connected into a 3D architecture, denoted as MOF-Calix (Fig. 2).[25] MOF-Calix crystallizes in the triclinic space group $P\bar{1}$ and shows two crystallographic independent Cd atoms. The Cd1 atom adopts an octahedral coordination geometry and is six-coordinated by four O atoms of the carboxylate groups from 5-NO_2-BDC and two N atoms from the calix[4]arene ligand. The Cd2 atom also takes an octahedral coordination geometry, coordinated by four O atoms of the carboxylate groups from 5-NO_2-BDC, one O atom from MeOH and one N atom from one calix[4]arene ligand, leaving in the 2D layer an uncoordinated N atom of the pyridine group from tetra-pyridyl-functionalized calix[4]arene. Since the 3D bulk material is integrated by the 2D layer array, the authors transformed MOF-Calix through a simple and easy exfoliation process where the 2D layers are separated into ultrathin single (2.20 nm) or double-layer (3.73 nm) 2D MOF-Calix nanosheets. Apparently, taking advantage of the host–guest interaction pro-

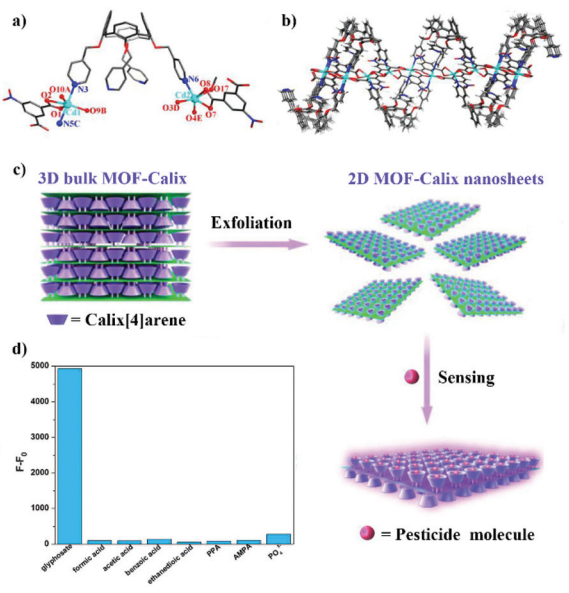

Fig. 2 (a) View of the coordination environment of the Cd centers in MOF-Calix. (b) View of the 2D structure in MOF-Calix extending along the *bc* plane. (c) Schematic illustration of the fabrication of 2D MOF-Calix nanosheets and sensitive detection of pesticides through host–guest chemistry. (d) The fluorescence response of the MOF-Calix nanosheets towards various organic acids and PO_4^{3-} (45 μM for each). Adapted with permission from ref. 25 copyright (2020) Elsevier.

vided by calix[4]arene, the cavities were able to self-adjust to better incorporate glyphosate molecules by varying their size and shape as the pyridine group from calix[4]arene could freely rotate *via* the methylene groups. As the glyphosate molecules were immobilized in the host of calix[4]arene by the host–guest interaction, the rigidity of the backbone was amplified, facilitating the electron transfer through a radiative decay process after the photoexcitation process, increasing the fluorescence intensity.[25] The selectivity of MOF-Calix was explored by competition of plenty inorganic ions as well of additional carboxylic and phosphonic acid compounds (formic acid, acetic acid, benzoic acid, ethanedioic acid, phenylphosphonic acid (PPA), (amino-methyl)phosphonic acid (AMPA) and PO_4^{3-}). Under the same experimental conditions, no noticeable interference nor fluorescence variation was observed for these analytes. To find out whether the guest size played a decisive role in the selective sensing or not, the fluorescence intensity of MOF-Calix nanosheets was determined in the presence of organic molecules with a similar size to glyphosate: glutaric acid and iminodiacetic acid. After adding a solution of 45 μM glutaric acid and iminodiacetic acid independently, the fluorescence intensity increased by 6.3% and 10.9% respectively, while for glyphosate 240% fluorescence enhancement was observed emphasizing its selectivity for glyphosate with a detection limit of 2.25×10^{-6} M.[25]

Moreover, azinphos-methyl, a widely employed OPP to control many insect pests on a variety of fruits, vegetables, nuts, grapes, apples, crop fields and shade trees, and a key ingredient in the preparation of several commercially available pesticides, was analyzed in real samples from the extract of apples[59,60] and tomatoes[59] by Singha's group. Two different compounds derived from the same metal ion (Cd(II)) and ligand (1,4-phenylenediacetic acid (PDA) and 1,2,4-triazol (tz)) were studied.[59,60] $[Cd_{2.5}(PDA)(tz)_3]n$ was the product from the solvothermal reaction,[60] whilst $[Cd_3(PDA)(tz)_3Cl(H_2O)_4]\cdot 3H_2O$ was obtained from the reaction at room temperature with minor solvent changes.[59] The first one is a 3D MOF with an asymmetric unit integrated by one PDA, three tz and two and a half crystallographically independent Cd(II) ions. The coordination environment of Cd1 plays an important role in the recognition as this central ion has an unsaturated coordination vacancy in a distorted trigonal bipyramidal geometry. The authors suggest that the π···π interactions along with this vacancy are both responsible for the detection of azinphos-methyl (Fig. 3).[60] On the other hand, although $[Cd_3(PDA)(tz)_3Cl(H_2O)_4]\cdot 3H_2O$ is also a 3D MOF, its asymmetric unit consists of one PDA, three tz, one chloride ion, four coordinated water molecules, three lattice water molecules and three crystallographically independent Cd(II) ions, where all the Cd(II) ions have a distorted octahedral geometry. As a consequence, the interaction with the OPPs is limited by the π···π interactions solely.[59] Both of the coordination frameworks exhibited a turn-off response for the azinphos-methyl pesticide. The evaluation of the interference and competition with other OPPs were carried out with the simultaneous existence of parathion, chlorpyrifos, diazinon, endosulfan, malathion and

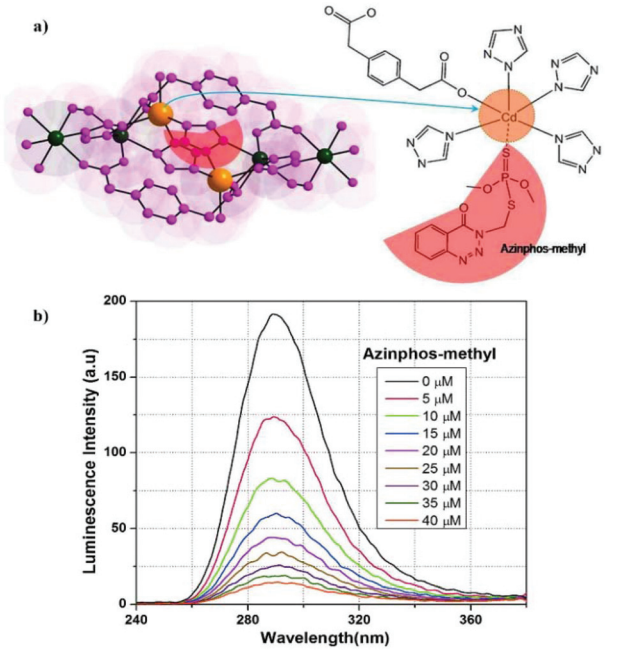

Fig. 3 (a) Schematic of five coordinated Cd(II) ions (Cd1-Orange) and the proposed coordination interaction of azinphos-methyl through the S atom inside the cage. (b) Emission spectra of 1 dispersed in water upon incremental addition of the acetonitrile solution of azinphos-methyl (λ_{ex} = 225 nm). Adapted with permission from ref. 60 copyright (2020) Wiley Online Library.

dichlorvos in water, resulting in an exclusive quenching for azinphos-methyl by $[Cd_{2.5}(PDA)(tz)_3]n$; meanwhile, the solvothermal product showed 90%, 52%, and 49% luminescence quenching for azinphos-methyl, chlorpyrifos, and parathion respectively.[60] Probably, this phenomenon was caused by the absence of unsaturated coordination sites in the network, even though no further explication was given. Additionally, the LOD of the room temperature product is lower than that of the solvothermal product (25×10^{-9} M and 5×10^{-5} M).[59,60] As both systems show the same emission band (derived from the PDA ligand) and both detect azinphos-methyl, the quenching mechanism has been attributed to the absorption of the excitation light from the MOF to the azinphos-methyl molecule in a resonance energy transfer process which is in congruence with the UV-spectra of the sensors and target molecule.[59]

Besides OPPs, organochlorine pesticides (OCPs) constitute another significant division of hazardous pollutants in anthropogenic activities (Scheme 3). 2,6-Dichloro-4-nitroaniline (DCN) is found to be one of the most important and widely used pesticides for protecting crops from various diseases such as fruit trees, cotton rotten bells and wheat powdery mildew.[24,37,63] Nevertheless, its high toxicity, slow degradation rate and insoluble properties cause severe damage to living organisms, and it can enter the human body through the skin and lungs. Also, its absorption through the gut wall affects the central nervous system leading to convulsions, hyper-reflexia, ataxia and tremor, and it is even suspected to be a

carcinogen.[24,37,63] Hence, Zhang's group has developed an interesting enantiomeric chiral pair of CPs based on the chiral ligand (1*R*,2*R*/1*S*,2*S*)-2,2′-((5-carboxy-1,3-phenylene)bis(oxy)) dipropionic acid ((1*R*,2*R*/1*S*,2*S*)-Hcpba), phenantroline (phen) and cadmium (Fig. 4).[62] Obviously, since the enantiomeric pair is isomorphic, only $[Cd_2((1S,2S)\text{-Hcpba})_2(phen)_2]n$ was described.[62] The crystalline compound belongs to the $P2_1$ space group, and the asymmetric unit contains two Cd(II) ions, two (1*S*,2*S*)-Hcpba and two phen as ligands. The metallic ion is located at the center of a twisted octahedron defined by four O atoms from three different (1*S*,2*S*)-Hcpba, and two chelating N atoms from the phen molecule.[62] As has been observed, the use of 2,2′-bipyridine type ligands[80] is usually limited in coordination polymers with low dimensionality (1D). Yet, attention-grabbing properties like circular dichroism (with a negative Cotton effect at 275 nm) and the luminescence recognition of pesticides, antibiotics and chiral nitroaromatic analytes were studied. The most remarkable achievement for the pesticide detection was the selective quenching response for DCN (LOD = 3.79×10^{-7} M) with negligible interference from glufosinate, glyphosate, 2,4-dichlorophenol and atrazine in DMF.[62] The turn-off behavior was explained by the combination of PET and FRET mechanisms supported by electrochemical data and UV-vis spectra. Nonetheless, the enantiomeric recognition by the pair of chiral CPs in chiral nitroaromatic molecules was unsuccessful, as both the CPs could not discriminate between the nitroaromatic enantiomers.[12,62]

Similarly, the 3D MOF $(H_3O)[Zn_2L(H_2O)]\cdot 3NMP\cdot 6H_2O$ (L = 2,5-(6-(4-carboxyphenylamino)-1,3,5-triazine-2,4-diyldiimino) diterephthalic acid) is also capable of detecting DCN.[24] This particular MOF crystallized in the space group $P2_12_12_1$ with a 4-connected 3D framework. The negative charge of the framework was balanced with H_3O^+. Two crystallographically independent zinc ions are part of the asymmetric unit and both metallic ions adopted a distorted tetrahedral geometry with four atoms of oxygen provided by three carboxylate ligands constructing a relatable Zn paddlewheel SBU in the network (Fig. 5).[24] Curiously, $(H_3O)[Zn_2L(H_2O)]\cdot 3NMP\cdot 6H_2O$ shows a distinctive luminescence performance against some pesticides. Strong quenching is shown in the presence of DCN and trifluralin (TFL); however, its selectivity was achieved through a unique bathochromic shift of 43 nm after the addition of TFL that can even be appreciated under naked-eyed conditions. Still, a higher sensitivity for DCN was achieved with a lower detection limit (4.76×10^{-9} M). The quenching mechanism considers the electron-withdrawing nature of the $-NO_2$ and

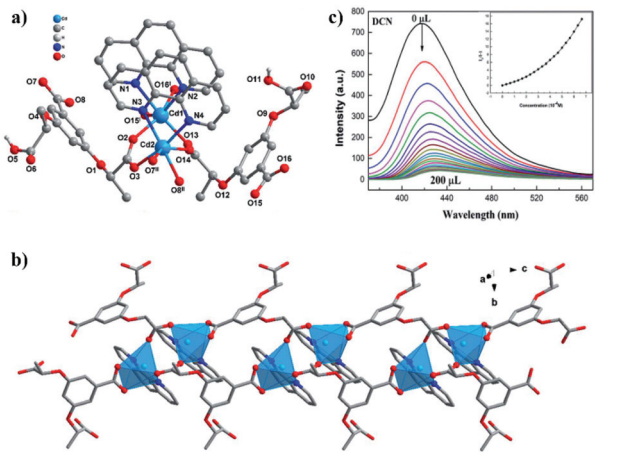

Fig. 4 (a) Stick–ball representation of the structural unit of $[Cd_2((1S,2S)\text{-Hcpba})_2(phen)_2]n$. (b) 1D-chain structural representation along the *c* axis. (c) Luminescence spectra and the SV plots with DCN (10 mM, 10 mL addition each time). Adapted with permission from ref. 62 copyright (2020) The Royal Society of Chemistry.

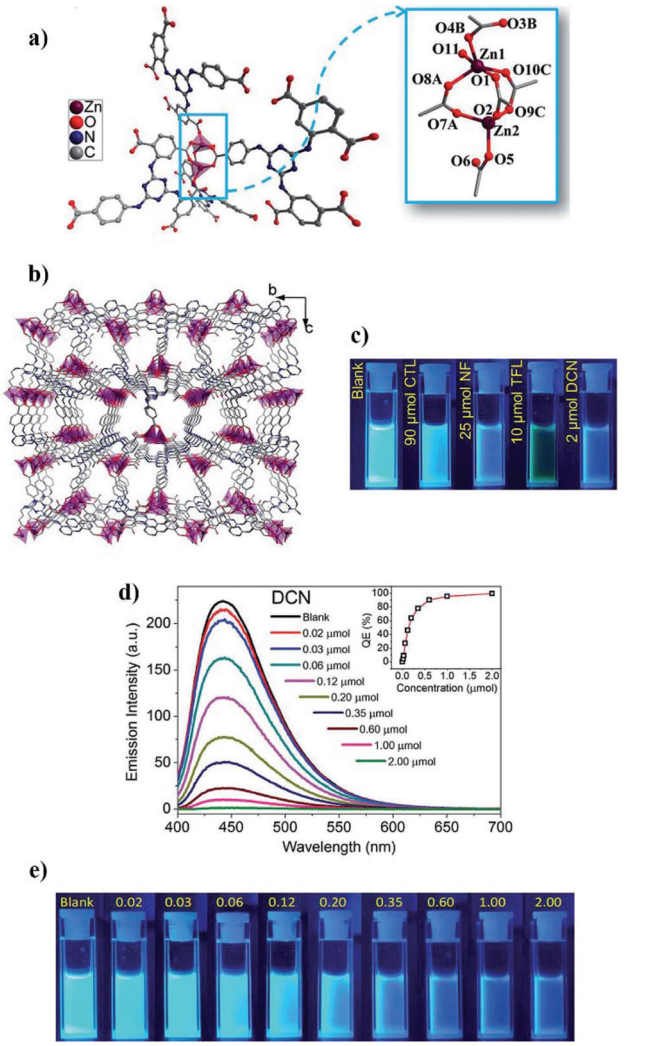

Fig. 5 (a) The coordination environment of the binuclear Zn(II) centers of $(H_3O)[Zn_2L(H_2O)]\cdot 3NMP\cdot 6H_2O$. (b) The 3D framework observed along the *a* axis. (c) Fluorescence variation of $(H_3O)[Zn_2L(H_2O)]\cdot 3NMP\cdot 6H_2O$ with trace addition of pesticides under 365 nm UV light. (d) Concentration-dependent fluorescence responses of $(H_3O)[Zn_2L(H_2O)]\cdot 3NMP\cdot 6H_2O$ at different concentrations of DCN (λ_{ex} = 365 nm) inset: luminescence quenching efficiency (QE) *versus* addition concentration of DCN. (e) Fluorescence variations with step-by-step addition of DCN (mmol) under 365 nm UV light. Adapted with permission from ref. 24 copyright (2020) The Royal Society of Chemistry.

–CF_3 groups in the energy level calculations by density functional theory, converging in the synergistic effect of the PET and FRET processes.[24]

Correspondingly, DCN has been detected in real samples as well. The 3D MOF $[Zn_3(DDB)(DPE)]\cdot H_2O$ (DDB = 3,5-di(2′,4′-dicarboxylphenyl)benzoic acid and DPE = 1,2-di(4-pyridyl) ethylene) has accomplished the fluorescence recognition of DCN in extracts from carrots, nectarines and grapes.[37] The analysis of the crystal structure reveals that the framework crystallizes in the $P2_1/c$ space group. Its asymmetric unit contains three Zn(II) ions, one μ_3-OH^- ion, one DPE and one DDB ligand. Three Zn(II) ions are connected by one μ_3-OH^- ion and four carboxylate groups to form a trinuclear $[Zn_3(OH)(COO)_4]$ cluster. Then, two trinuclear clusters are linked by two carboxylate groups to form a six-nuclear $[Zn_6(OH)_2(COO)_{10}]$ cluster constructing a 4,12-connected net (Fig. 6).[37] Thus, the DCN fluorescence sensing was explored among other eight OCPs.[37] Non-significant changes except for the notorious quenching from DCN were revealed. The quenching efficiency in the DCN detection scales up to 93.5% with a limit of detection equal to 2.7×10^{-7} M in water. These favorable results allowed the determination of DCN by the MOF in the above-mentioned fruits and vegetables. It is worth noting that the turn-off mechanism was studied with the assistance of computational chemistry concluding in a PET process caused by the electron-withdrawing –NO_2 group.[37]

In an interesting methodology for the luminescence recognition of Nitenpyram, Yang *et al.*[64] have incorporated fluorescent guest molecules in the $[Cd_2(tib)(btb)(H_2O)_2]\cdot NO_3\cdot 2.5DMF$[92] MOF with the intention to create a dual-emitting platform system. Rhodamine B (Rho B) and Rhodamine 6G (Rho 6G) were the guest molecules selected.[64] X-Ray crystallographic analysis revealed that the MOF crystallized in the space group $P2_12_12_1$. The asymmetric unit consists of two Cd(II) ions, one tib ligand, one btb ligand, two coordination water molecules, one NO_3^- and two and a half DMF molecules. Each Cd(II) ion has a diverse coordination environment. Cd1 is seven-coordinated by five O atoms from three btb ligands, one O atom from one coordination H_2O molecule and one N atom from one tib ligand, whereas Cd2 has a distorted octahedral geometry integrated by three O atoms from three different btb ligands, one O atom from one coordinated H_2O molecule and two N atoms. A binuclear {Cd2} unit is formed through the carboxylate groups of btb ligands, and subsequently, these binuclear units are connected by the tib ligand constructing a 3D network with empty one dimensional channels, having an effective pore volume of 53% (3417 Å^3) per unit cell (6514 Å^3) calculated by the PLATON program.[92] The loaded MOF with the guest molecules shows two main emissions at 370 nm and approximately 600 nm, respectively. The emission at 370 nm originated from the MLCT, while the emission at approximately 600 nm comes directly from the dye molecules of rhodamine B or 6G.[64] Both the dual-emitting systems have been applied in the sensing of nitenpyram, thiamethoxam, cypermethrin, carbaryl and rotenone. Changes in the fluorescence intensity were observed with the following quenching efficiency: nitenpyram > thiamethoxam > cypermethrin ≈ carbaryl > rotenone. This tendency is equally valid for both systems independent of the type of rhodamine guest in the MOF. For Rho B@MOF the detection limit was estimated to be 4.8×10^{-10} M, while 3×10^{-9} M was the corresponding value for Rho 6G@MOF. Remarkably, each system has distinctive dual emission behavior (Fig. 7). The extinguishing of the fluorescence properties was explained by computing the HOMO and LUMO energies of the five pollutants by applying density functional theory agreeing in a PET process.[64]

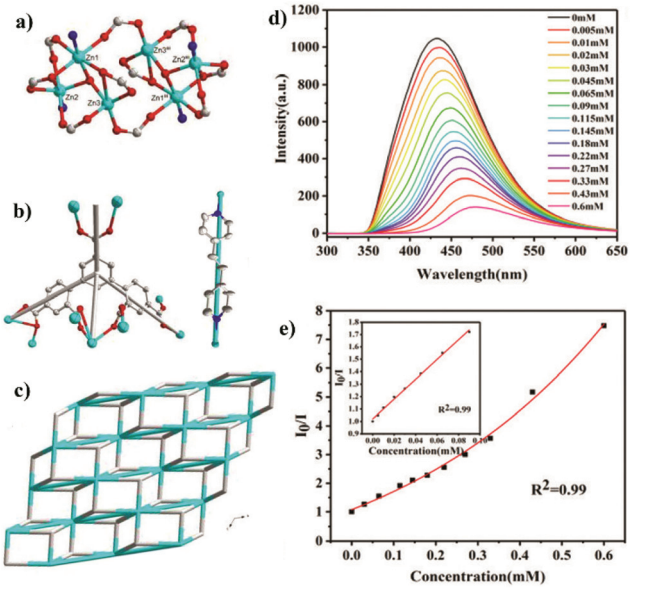

Fig. 6 (a) SBU in $[Zn_3(DDB)(DPE)]\cdot H_2O$ MOF (b) Linkage mode of the DPE and DDB ligands. (c) Simplified representation of the network in $[Zn_3(DDB)(DPE)]\cdot H_2O$ along the *b* axis. (d) Fluorescence spectra of the MOF at different concentrations of DCN in aqueous solution including 100 μL carrot extract. (e) Stern–Volmer plot for the detection of DCN in aqueous solution including 100 μL carrot extract. Inset: linear fitting part. Adapted with permission from ref. 37 copyright (2020) The Royal Society of Chemistry.

CPs and MOFs as fluorescent sensors of herbicides and the cyanide ion

Simazine is a frequently used general-purpose herbicide considered as a toxic contaminant with potential endocrinal disrupting activity (Scheme 4).[65] Vasylevskyi's group has employed the 2D coordination polymer $\{[Cd(\mu_2\text{-}BA)_2(ClO_4)_2]\cdot n(DCM)\}n$ (BA = bis-9,10-(pyridine-4-yl)-anthracene) as a fluorescent sensor for the detection of simazine.[65] $\{[Cd(\mu_2\text{-}BA)_2(ClO_4)_2]\cdot n(DCM)\}n$ is one of the series of Zn and Cd CPs connected through the BA ligand. Structural differences in those coordination polymers (beside the metallic ions and crystallization solvent molecules) arise according to the counter-ion responsible for the charge balance. However, among all the anions that lead to the synthesis of the CPs, the use of ClO_4^- as a counter-ion directed the construction to the

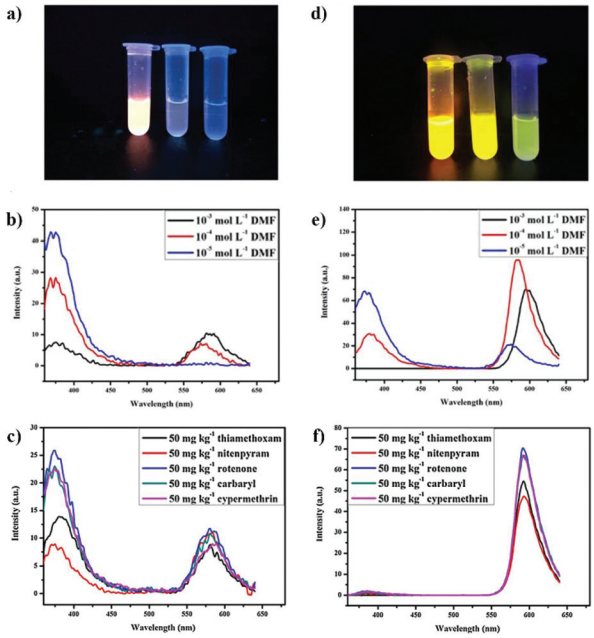

Fig. 7 (a) Photograph of the changes in solution colors under UV light (365 nm) according to the concentration in the "(b) plot" for Rho B@MOF in DMF. (b) Emission spectra of Rho B@MOF in DMF. (c) Fluorescence intensity of Rho B@MOF with different pesticides at 50 mg kg^{-1}. (d) Photograph of the changes in solution colors under UV light (365 nm) according to the concentration in the ("e) plot" for Rho 6G@MOF in DMF. (e) Emission spectra of Rho 6G@MOF in DMF. (c) Fluorescence intensity of Rho 6G@MOF with different pesticides at 50 mg kg^{-1}. Adapted with permission from ref. 102 copyright (2020) Elsevier.

most porous framework with potential host–guest interaction (cages of 11.2 × 11.2 Å). The cadmium CP crystallizes in the monoclinic space group *C*2/*c*. The central ion has a distorted coordination geometry occupied by four N-atoms from the BA ligand in the equatorial positions. Axial positions are fulfilled by the ClO_4^- ions. The BA ligand acts a bridge assembling the two-dimensional net. The interaction of simazine with $\{[Cd(\mu_2\text{-}BA)_2(ClO_4)_2]\cdot n(DCM)\}n$ in MeCN provides a turn-off response in the luminescence properties (LOD = 4.783 × 10^{-7} M).[65] Thus, an exclusive selectivity could not be achieved since the CP also exhibited strong quenching for 2,4,6-trichloroanisole (TCA) (and for other nitrocompounds) under the same conditions.[65] Nevertheless, TCA is a secondary product from the microbial action on trichlorophenol used as a fungicide; although it has not been considered particularly toxic for humans, it is responsible for the appearance of corked wine fault in wines. The detection limit for TCA was as well calculated to be up to 6.13 × 10^{-8} M.[65]

Beyond organochlorine herbicides, "quats" have gained tremendous attention as nonselective and quick-acting weed killers.[67] The term quat comes from dicationic molecules containing a diquaternary bipyridyl motif, *e.g.* 1,1′-Dimethyl-4,4′-bipyridinium ((PQ) or paraquat), 6,7-dihydrodipyrido[1,2-*a*2′,1′-*c*]pyrazinediium ((DQ) or diquat), 1,1′-di-methyl-2,2′-bipyridinium (OQ), (Scheme 4) and 1,1′-bis(3,5-di-*tert*-butyl-benzyl)-4,4′-bipyridinium (TBPQ).[67] Its mechanism of action involves the quat species as an electron acceptor available from the plant photosynthetic system I (PSI), leading to the generation of radicals, which in turn react with molecular oxygen disrupting the photosynthetic process. In the case of humans, it is known that the direct exposure to PQ results in dangerous health consequences, which may include pulmonary fibrosis, pulmonary edema, erythema, dermatitis, mouth ulceration, kidney failure and brain damage.[67] In general, quats are considerably toxic and do not have a specific antidote.[68] Conveniently, Mukhopadhyay's group has designed a selective fluorescent "Zn-DBC" MOF capable of distinguishing between the dicationic bipyridinium salts, accordingly to its size and redox properties (Fig. 8).[67] The $[Zn_{1.5}(DBC)\cdot(H_2O)\cdot(DMF)\cdot Me_2NH_2]n$ crystals belong to the *Pbcn* space group. The asymmetric unit was found to contain 1.5 Zn(II) ions, one DBC linker, H_2O and DMF as crystallization molecules and one dimethylammonium (DMA) cation as a counter-ion for the charge balance in the anionic framework. This special feature allowed the 3D MOF to undergo a post-synthetic cation exchange with the dicationic quats. For this purpose, PQ, DQ, OQ, and TBPQ were investigated.[67] It is important to mention that the exchange process as well the luminescence studies occurred in water solution. A gradual decrease in the fluorescence intensity was observed for all the bipyridyl dications; however, DQ stood out from the rest. The authors justify the selectivity for diquat through the calculation of the reduction potential for all the series against the saturated calomel electrode (SCE) reference. The tendency goes as: OQ(−0.60 V) < PQ

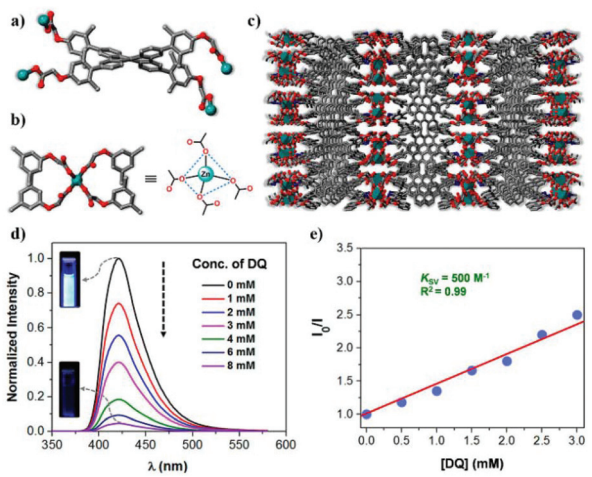

Fig. 8 (a) The coordination modes of the carboxylate groups of DBC and (b) the tetrahedral coordination environment of Zn(II) in Zn-DBC. (c) Crystal packing diagram of Zn-DBC down the *c* axis; note that Zn, O, and N atoms are represented in cyan, red, and blue, respectively. (d) Quenching of the fluorescence intensity of Zn-DBC with increasing concentration of DQ(PF6)2 in water (λ_{ex} = 350 nm) at rt. Note the changes in the fluorescence images (insets) of the aqueous dispersion of the MOF before and after quenching titration. (e) Corresponding Stern–Volmer quenching plot with increasing concentration of DQ. Adapted with permission from ref. 67 copyright (2020) American Chemical Society.

(−0.45 V) < TBPQ(−0.37 V) < DQ(−0.35 V). Unsurprisingly, DQ showed the lowest fluorescence intensity (according to the PET mechanism), as PQ and OQ followed the expected behaviour. TBPQ, on the other hand, showed almost no turn-off effect in the luminescent material. Here is where the size comes to place. Due to the highly hindered *tert*-butyl groups of TBPQ, its transportation to the accessible voids in the crystal was more difficult minimizing its interaction with the MOF, highlighting its size-selective character. The LOD for diquat was estimated to be 1.52×10^{-5} M.[67] An honorific mention corresponds to the NKU-101 [93] MOF, where, in an almost identical manner, this anionic framework suffered from the post-synthetic cation exchange of diethylammonium with PQ. Nonetheless, the PQ determination was only carried out by the UV-Vis technique.[93]

Quats fluorescence recognition is not limited exclusively to anionic frameworks, neutral frameworks such as $[Zn_2(cptpy)(btc)(H_2O)]n$ (cptpy = 4-(4-carboxyphenyl)-2,2′:4′,4″-terpyridine; btc = 1,3,5-benzenetricarboxylic acid) has proved its competence as well.[68] The Zn-MOF crystallized in the $P2_1/c$ space group. Two crystallographically independent Zn(II) ions, one coordinated water molecule, one cptpy ligand and one btc ligand integrated the asymmetric unit. The two Zn(II) ions showed different coordination geometries. Zn1 shows a tetrahedral environment, whilst the geometry of Zn2 is defined as a pentacoordinate square pyramid. One-dimensional chains are generated by adjacent Zn1 and Zn2 atoms alternately connected through btc ligands. At the same time, the neighboring Zn1 and Zn2 atoms were bridged by cptpy ligands to form 2D layers. As a result, the 1D chains and 2D layers were inter-connected with each other to produce a 3D framework with 1D channels in all three directions.[68] The luminescence intensity of $[Zn_2(cptpy)(btc)(H_2O)]n$ weakened almost completely after the addition of PQ in water solution. Unfortunately, no further herbicide or pesticide was analyzed to appreciate the complete discriminatory potential against these pollutants. The quenching mechanism could have occurred by a PET process since the UV-Vis absorption spectra of PQ show a large overlap with the excitation spectrum of the MOF. Moreover, the authors suggested that hydrogen bonds and interactions could also be responsible for quenching.[68]

Alongside pesticides and herbicides, it is one of our deepest interest to enrich the luminescence detection of environmental hazardous compounds by complementing the ion sensing reported previously in the relevant literature[20,27,28] with the scarcely mentioned cyanide ion. Compared to the very toxic heavy-metal ions, CN^- can lead to the death of humans and aquatic life in minutes. The lethal effect of cyanide in physiological systems lies in the inhibition of respiration in the mitochondrial respiratory chain, occasioned by the cyanide binding to the Fe^{3+} ion of cytochrome oxidase, affecting the normal functioning of the lungs and brain.[69,70] Nowadays, the luminescence recognition of the CN^- ion by applying coordination framework materials is still very rare.[35] Nevertheless, recent achievements have come to light in three distinctive compounds based on Zn(II) ions. The first one is a one-dimensional CP with the formula $\{[Zn_2(H_2O)_2(e,a\text{-}cis\text{-}1,4\text{-}chdc)_2(4,4'\text{-}dtbb)_2]\cdot 7H_2O\}n$, 1,4-chdc = 1,4-cyclohexanedicarboxylato, 4,4′-dtbb = 4,4′-di-*tert*-butyl-2,2′-bipyridine, which crystallizes in the *Pn* space group with two Zn(II) ions, two *e*,*a*-*cis* 1,4-chdc, two 4,4′-dtbb, two aqua ligands, and seven lattice water molecules in its asymmetric unit. The two crystallographically different Zn(II) ions have a distorted octahedral configuration with a similar coordination environment surrounded by four oxygen atoms from two different 1,4-chdc ligands and the aqua ligand, and two nitrogen atoms from one 4,4′-dtbb. Each 1D polymer chain is formed as a result of the combined monodentate η^1 and chelate bidentate η^2 coordination modes of 1,4-chdc, along with the *e*,*a*-*cis* conformation of its carboxylate groups connecting the metal centers in a characteristically V-shaped fashion (Fig. 9). Simultaneously, both 1D chains are attached together by several hydrogen bonds from the lattice water molecules. The presence of competing anions (F^-, Cl^-, Br^-, I^-, AcO^-, NO_3^-, NO_2^-, $H_2PO_4^-$, $H_3P_2O_7^-$, HCO_3^-, $H_2AsO_4^-$ and SO_4^{2-}) displays almost an exclusive prominent turn-off response for the cyanide ion in pure water at different pH values (LOD = 9×10^{-8} M in pH = 7.0). The explanation behind this quenching behavior was attributed to the displacement of the ligands in the CP for the cyanide ion to form $Zn(CN)_2$, which was demonstrated by IR and SEM techniques with the solid residue, while in the aqueous phase the presence of the ligands was verified by ^1H NMR and MS-ESI(+) methods.[71]

Alternatively, Ghosh *et al.* have focused on the post-synthetically modifications of ZIF-90 and bio-MOF-1 for the cyanide

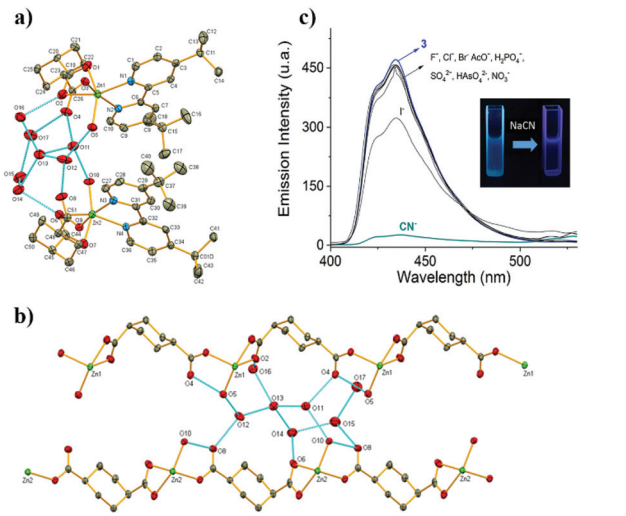

Fig. 9 (a) Supramolecular dinuclear repeating unit of $\{[Zn_2(H_2O)_2(e,a\text{-}cis\text{-}1,4\text{-}chdc)_2(4,4'\text{-}dtbb)_2]\cdot 7H_2O\}n$ (ellipsoids shown at 60% probability); hydrogens are omitted for clarity. (b) 1D V-shaped dual-polymer chain of $\{[Zn_2(H_2O)_2(e,a\text{-}cis\text{-}1,4\text{-}chdc)_2(4,4'\text{-}dtbb)_2]\cdot 7H_2O\}n$; hydrogens and 4,4′-dtbb ligands are omitted for clarity. (c) Photoluminescence spectral changes of the CP upon addition of 10 equiv. of different anions. The inset shows a picture taken under irradiation with 365 nm UV light in the absence and presence of CN^-. Adapted with permission from ref. 71 copyright (2020) The Royal Society of Chemistry.

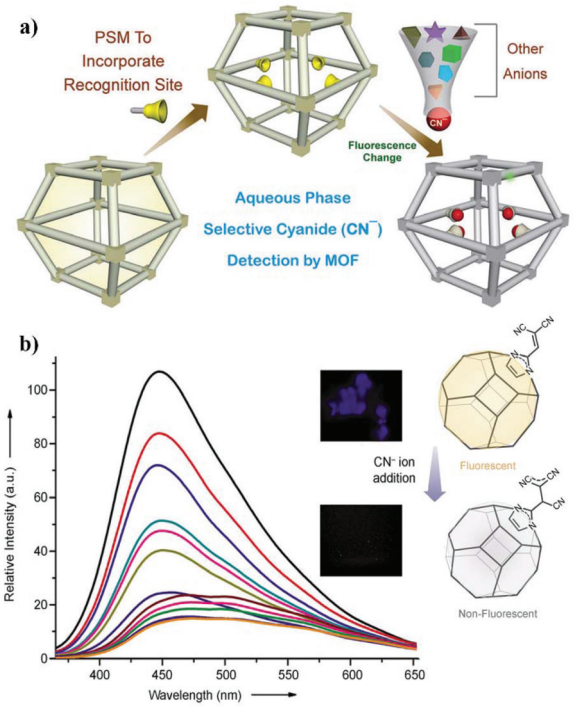

Fig. 10 (a) Schematic overview of the post-synthetic modification in the MOF leading to the selective sensing of the cyanide ion. (b) Fluorescence response of M-ZIF-90 upon incremental addition of CN^- ions showing a turn-off response. The inset shows confocal images before and after the addition of CN^-. Adapted with permission from ref. 69 copyright (2016) Wiley Online Library.

sensing.[35,69,70] In the particular case of ZIF-90 (Fig. 10),[69] as the structure possesses an aldehyde group aligned within the pores of the extended 3D sodalite framework, the ZIF undergoes a Knoevenagel reaction with malononitrile, transforming the aldehyde group into a dicyanovinyl group with the retention of crystallinity (M-ZIF-90).[69] Herein, the dicyanovinyl group undergoes a nucleophilic addition of cyanide, resulting in a significant quenching effect, justified by the loss of conjugation in the dicyanovinyl group and also supported by the electronic potential maps of the LUMO and HOMO energy states of the ligand. Furthermore, no interference from other anions was observed as F^-, Cl^-, Br^-, N_3^-, SCN^-, NO_3^- and NO_2^- were analysed in DMSO–H_2O (1 : 1) medium.[69] A different strategy was followed for the corresponding bio-MOF-1. Due to its inherent 3D anionic porous architecture, successive cation exchange between dimethylammonium, 3,6-diaminoacridinium (DAAC) and tetrabutylammonium (TBA) was successfully attempted. In the first stage, the original counter-ion in bio-MOF-1 (DMA) was switched by the cationic dye DAAC. Once loaded in the MOF, DAAC is susceptible to attack by the nucleophilic cyanide ion of the TBACN salt, *via* Michael type addition, rendering a neutral dye and once again exchanging the counter-ion DAAC for TBA. The release of the neutral cyanide containing dye promotes the turn-on response in the fluorescence with great selectivity, and even *in vitro* studies could be performed with human breast cancer cell lines (MCF-7), monitoring the trace of cyanide inside the cytoplasm with a limit of detection equal to 1.9×10^{-8} M.[35]

Significantly, other luminescent coordination frameworks have turned their focus on the recognition of pesticides, herbicides and the cyanide ion and those valuable contributions are listed in Table 1.

Conclusions

At times where the vulnerability of humans due to dangerous biomolecules or chemical substances is evident, it is of the upmost necessity to continue developing functional compounds and materials with synergy among their chemical, structural and optical properties to become sensitive instant probes aimed at the detection of these unwanted compounds. Hence, Zn(II) and Cd(II) CPs and MOFs are at the forefront as luminescent sensors due, mainly, to their straightforward synthesis, and also due to their crystalline and modifiable structures, which by simply tuning the ligands' chemical nature, can favour optical and textural (*i.e.*, porosity) properties effective in chemosensing through host–guest interactions.

Moreover, many luminescent Zn and Cd coordination arrays have been demonstrated to be stable enough for convenient, affordable, sensitive, and sometimes selective and reusable, immediate sensing of divergent analytes both in water and organic solvent media. Although new substitute less-toxic chemicals can be developed and stricter environmental regulations can be implemented, without doubt, poisonous chemicals such as pesticides, herbicides and cyanide, will be around us for some time, demanding, at least, facile, rapid and low-cost detection of those substances. Therefore, the advancement in the design of novel luminescent Zn and Cd coordination arrays that can be stable predominantly in the aqueous environment is gaining relevance since water sources around the world are frequently, and increasingly, polluted with these types of hazardous and toxic compounds.

Finally, it is also significant to be aware of those opening areas of research that this topic offers, among them perhaps the more appealing are the following: thorough studies of the mechanisms behind the photoluminescence sensing phenomena, using in cooperation empirical and theoretical approaches; the creation of new Zn and Cd coordination networks with the capability of high sensitivity and, most importantly, selectivity towards a certain substance or analyte.

In a nutshell, the development of sensitive, selective and reusable Zn and Cd luminescent chemosensors can provide new directions toward real-time detection and quantification of industrially and environmentally relevant molecules with real-life applications.

Conflicts of interest

There are no conflicts to declare.

Acknowledgements

VSM thanks Universidad Autónoma del Estado de México for funding (Project: 6171/2020CIB). The authors thank UNAM (DGAPA-PAPIIT-216220). LDRV thanks CONACyT for the PhD scholarship (713164).

Notes and references

1 S. Kitagawa and R. Matsuda, *Coord. Chem. Rev.*, 2007, **251**, 2490–2509.
2 W. L. Leong and J. J. Vittal, *Chem. Rev.*, 2011, **111**, 688–764.
3 X. Zhang, W. Wang, Z. Hu, G. Wang and K. Uvdal, *Coord. Chem. Rev.*, 2015, **284**, 206–235.
4 M. Mon, R. Bruno, J. Ferrando-Soria, D. Armentano and E. Pardo, *J. Mater. Chem. A*, 2018, **6**, 4912–4947.
5 W. P. Lustig, S. Mukherjee, N. D. Rudd, A. V. Desai, J. Li and S. K. Ghosh, *Chem. Soc. Rev.*, 2017, **46**, 3242–3285.
6 H. L. Nguyen, C. Gropp and O. M. Yaghi, *J. Am. Chem. Soc.*, 2020, **142**, 2771–2776.
7 X. Cai, Z. Xie, D. Li, M. Kassymova, S. Q. Zang and H. L. Jiang, *Coord. Chem. Rev.*, 2020, **417**, 213366.
8 S. R. Batten and K. S. Murray, *Coord. Chem. Rev.*, 2003, **246**, 103–130.
9 E. Loukopoulos and G. E. Kostakis, *J. Coord. Chem.*, 2018, **71**, 371–410.
10 K. A. Cychosz, A. G. Wong-Foy and A. J. Matzger, *J. Am. Chem. Soc.*, 2008, **130**, 6938–6939.
11 J. Duan, W. Jin and S. Kitagawa, *Coord. Chem. Rev.*, 2017, **332**, 48–74.
12 J. Heine and K. Müller-Buschbaum, *Chem. Soc. Rev.*, 2013, **42**, 9232–9242.
13 A. Erxleben, *Coord. Chem. Rev.*, 2003, **246**, 203–228.
14 A. M. Cheplakova, K. A. Kovalenko, D. G. Samsonenko, A. S. Vinogradov, V. M. Karpov, V. E. Platonov and V. P. Fedin, *CrystEngComm*, 2019, **21**, 2524–2533.
15 Y. S. Shi, Q. Q. Xiao, L. Fu and G. H. Cui, *CrystEngComm*, 2020, **22**, 4875–4886.
16 D. J. Tranchemontagne, J. L. Tranchemontagne, M. O′ keeffe and O. M. Yaghi, *Chem. Soc. Rev.*, 2009, **38**, 1257–1283.
17 A. Schoedel, M. Li, D. Li, M. O'Keeffe and O. M. Yaghi, *Chem. Rev.*, 2016, **116**, 12466–12535.
18 M. Ui, Y. Tanaka, Y. Araki, T. Wada, T. Takei, K. Tsumoto, S. Endo and K. Kinbara, *Chem. Commun.*, 2012, **48**, 4764–4766.
19 B. Parmar, K. K. Bisht, Y. Rachuri and E. Suresh, *Inorg. Chem. Front.*, 2020, **7**, 1082–1107.
20 T. Rasheed and F. Nabeel, *Coord. Chem. Rev.*, 2019, **401**, 213065.
21 H. Y. Li, S. N. Zhao, S. Q. Zang and J. Li, *Chem. Soc. Rev.*, 2020, **49**, 6364–6401.
22 K. Vikrant, D. C. W. Tsang, N. Raza, B. S. Giri, D. Kukkar and K. H. Kim, *ACS Appl. Mater. Interfaces*, 2018, **10**, 8797–8817.
23 L. Wang, K. He, H. Quan, X. Wang, Q. Wang and X. Xu, *Microchem. J.*, 2020, **153**, 104441.
24 L. Di, Z. Xia, J. Li, Z. Geng, C. Li, Y. Xing and Z. Yang, *RSC Adv.*, 2019, **9**, 38469–38476.
25 C. X. Yu, F. L. Hu, J. G. Song, J. L. Zhang, S. S. Liu, B. X. Wang, H. Meng, L. L. Liu and L. F. Ma, *Sens. Actuators, B*, 2020, **310**, 127819.
26 Y. Zhao, X. Xu, L. Qiu, X. Kang, L. Wen and B. Zhang, *ACS Appl. Mater. Interfaces*, 2017, **9**, 15164–15175.
27 S. Wu, H. Min, W. Shi and P. Cheng, *Adv. Mater.*, 2020, **32**, 1805871.
28 G. Liu, Y. Li, J. Chi, N. Xu, X. Wang, H. Lin, B. Chen and J. Li, *Dalton Trans.*, 2020, **49**, 737–749.
29 X. Y. Guo, Z. P. Dong, F. Zhao, Z. L. Liu and Y. Q. Wang, *New J. Chem.*, 2019, **43**, 2353–2361.
30 M. Li, D. Li, M. O'Keeffe and O. M. Yaghi, *Chem. Rev.*, 2014, **114**, 1343–1370.
31 X. Wang, C. Qin, E. Wang, Y. Li, N. Hao, C. Hu and L. Xu, *Inorg. Chem.*, 2004, **43**, 1850–1856.
32 K. Xing, R. Fan, S. Gao, X. Wang, X. Du, P. Wang, R. Fang and Y. Yang, *Dalton Trans.*, 2016, **45**, 4863–4878.
33 Y. Rachuri, K. K. Bisht, B. Parmar and E. Suresh, *J. Solid State Chem.*, 2015, **223**, 23–31.
34 M. Pamei and A. Puzari, *Nano-Struct. Nano-Objects*, 2019, **19**, 100364.
35 A. Karmakar, P. Samanta, S. Dutta and S. K. Ghosh, *Chem. – Asian J.*, 2019, **14**, 4506–4519.
36 L. Yang, Y. Song and L. Wang, *J. Mater. Chem. B*, 2020, **8**, 3292–3315.
37 X. Q. Wang, D. D. Feng, J. Tang, Y. Di Zhao, J. Li, J. Yang, C. K. Kim and F. Su, *Dalton Trans.*, 2019, **48**, 16776–16785.
38 Y. Li, D. Ma, C. Chen, M. Chen, Z. Li, Y. Wu, S. Zhu and G. Peng, *J. Solid State Chem.*, 2019, **269**, 257–263.
39 P. Kumar, A. Deep and K.-H. Kim, *TrAC, Trends Anal. Chem.*, 2015, **73**, 39–53.
40 T. Y. Gu, M. Dai, D. J. Young, Z. G. Ren and J. P. Lang, *Inorg. Chem.*, 2017, **56**, 4668–4678.
41 L.-T. Wu, Z.-J. Wang, X. Wu, C.-Y. Zhou, F. Su and C. Han, *Acta Crystallogr., Sect. C: Cryst. Struct. Commun.*, 2019, **75**, 141–149.
42 R. Goswami, S. C. Mandal, B. Pathak and S. Neogi, *ACS Appl. Mater. Interfaces*, 2019, **11**, 9042–9053.
43 P. Chandrasekhar, A. Mukhopadhyay, G. Savitha and J. N. Moorthy, *Chem. Sci.*, 2016, **7**, 3085–3091.
44 L. Zhang, Z. Kang, X. Xin and D. Sun, *CrystEngComm*, 2016, **18**, 193–206.
45 X. Zhang, X. Zhuang, N. Zhang, C. Ge, X. Luo, J. Li, J. Wu, Q. Yang and R. Liu, *CrystEngComm*, 2019, **21**, 1948–1955.
46 J. H. Qin, Y. D. Huang, M. Y. Shi, H. R. Wang, M. Le Han, X. G. Yang, F. F. Li and L. F. Ma, *RSC Adv.*, 2020, **10**, 1439–1446.
47 R. Dalapati and S. Biswas, *Sens. Actuators, B*, 2017, **239**, 759–767.
48 S. L. Jackson, A. Rananaware, C. Rix, S. V. Bhosale and K. Latham, *Cryst. Growth Des.*, 2016, **16**, 3067–3071.

49 J. Zhang, X. Zhang, J. Chen, C. Deng, N. Xu, W. Shi and P. Cheng, *Inorg. Chem. Commun.*, 2016, **69**, 1–3.
50 H. Zhang, J. Ma, D. Chen, J. Zhou, S. Zhang, W. Shi and P. Cheng, *J. Mater. Chem. A*, 2014, **2**, 20450–20453.
51 L. G. Qiu, Z. Q. Li, Y. Wu, W. Wang, T. Xu and X. Jiang, *Chem. Commun.*, 2008, 3642–3644.
52 C. Li, W. Yang, X. Zhang, Y. Han, W. Tang, T. Yue and Z. Li, *J. Mater. Chem. C*, 2020, **8**, 2054–2064.
53 X. Q. Yao, G. B. Xiao, H. Xie, D. D. Qin, H. C. Ma, J. C. Liu and P. J. Yan, *CrystEngComm*, 2019, **21**, 2559–2570.
54 Z. Liao, T. Xia, E. Yu and Y. Cui, *Crystals*, 2018, **8**, 338.
55 Y. M. Ying, C. L. Tao, M. Yu, Y. Xiong, C. R. Guo, X. G. Liu and Z. Zhao, *J. Mater. Chem. C*, 2019, **7**, 8383–8388.
56 Y. Liu, X. Y. Xie, C. Cheng, Z. S. Shao and H. S. Wang, *J. Mater. Chem. C*, 2019, **7**, 10743–10763.
57 P. Kumar, A. K. Paul and A. Deep, *Microporous Mesoporous Mater.*, 2014, **195**, 60–66.
58 P. Kumar, K. H. Kim, V. Bansal, A. K. Paul and A. Deep, *Microchem. J.*, 2016, **128**, 102–107.
59 D. K. Singha, P. Majee, S. Mandal, S. K. Mondal and P. Mahata, *Inorg. Chem.*, 2018, **57**, 12155–12165.
60 D. K. Singha, P. Majee, S. K. Mondal and P. Mahata, *ChemistrySelect*, 2017, **2**, 5760–5768.
61 J. C. Jin, Y. J. Zhu, J. Li, Y. L. Zhang and C. G. Xie, *Inorg. Chem. Commun.*, 2020, **119**, 108062.
62 L. Q. Zhang, X. W. Wang, L. Gu, Y. H. Yu and J. S. Gao, *RSC Adv.*, 2020, **10**, 9476–9485.
63 T. Kumar, M. Venkateswarulu, B. Das, A. Halder and R. R. Koner, *Dalton Trans.*, 2019, **48**, 12382–12385.
64 L. Yang, Y. L. Liu, C. G. Liu, F. Ye and Y. Fu, *J. Hazard. Mater.*, 2020, **381**, 120966.
65 S. I. Vasylevskyi, D. M. Bassani and K. M. Fromm, *Inorg. Chem.*, 2019, **58**, 5646–5653.
66 A. Mohanty, U. P. Singh, R. J. Butcher, N. Das and P. Roy, *CrystEngComm*, 2020, **22**, 4468–4477.
67 A. Mukhopadhyay, S. Jindal, G. Savitha and J. N. Moorthy, *Inorg. Chem.*, 2020, **59**, 6202–6213.
68 H. Chen, P. Fan, X. Tu, H. Min, X. Yu, X. Li, J. L. Zeng, S. Zhang and P. Cheng, *Chem. – Asian J.*, 2019, **14**, 3611–3619.
69 A. Karmakar, N. Kumar, P. Samanta, A. V. Desai and S. K. Ghosh, *Chem. – Eur. J.*, 2016, **22**, 864–868.
70 A. Karmakar, B. Joarder, A. Mallick, P. Samanta, A. V. Desai, S. Basu and S. K. Ghosh, *Chem. Commun.*, 2017, **53**, 1253–1256.
71 L. D. Rosales-Vázquez, J. Valdes-García, I. J. Bazany-Rodríguez, J. M. Germán-Acacio, D. Martínez-Otero, A. R. Vilchis-Néstor, R. Morales-Luckie, V. Sánchez-Mendieta and A. Dorazco-González, *Dalton Trans.*, 2019, **48**, 12407–12420.
72 X. Zheng, L. Zhou, Y. Huang, C. Wang, J. Duan, L. Wen, Z. Tian and D. Li, *J. Mater. Chem. A*, 2014, **2**, 12413–12422.
73 L. Wen, X. Xu, K. Lv, Y. Huang, X. Zheng, L. Zhou, R. Sun and D. Li, *ACS Appl. Mater. Interfaces*, 2015, **7**, 4449–4455.
74 N. C. Burtch, H. Jasuja and K. S. Walton, *Chem. Rev.*, 2014, **114**, 10575–10612.
75 J.-H. Wang, M. Li and D. Li, *Chem. Sci.*, 2013, **4**, 1793.
76 K. P. Kepp, *J. Phys. Chem. A*, 2019, **123**, 6536–6546.
77 V. Colombo, S. Galli, H. J. Choi, G. D. Han, A. Maspero, G. Palmisano, N. Masciocchi and J. R. Long, *Chem. Sci.*, 2011, **2**, 1311–1319.
78 M. D. Allendorf, C. A. Bauer, R. K. Bhakta and R. J. T. Houk, *Chem. Soc. Rev.*, 2009, **38**, 1330–1352.
79 J. Dong, D. Zhao, Y. Lu and W. Y. Sun, *J. Mater. Chem. A*, 2019, **7**, 22744–22767.
80 L. D. Rosales-Vázquez, V. Sánchez-Mendieta, A. Dorazco-González, D. Martínez-Otero, I. García-Orozco, R. A. Morales-Luckie, J. Jaramillo-Garcia and A. Téllez-López, *Dalton Trans.*, 2017, **46**, 12516–12526.
81 K. Müller-Buschbaum, F. Beuerle and C. Feldmann, *Microporous Mesoporous Mater.*, 2014, **216**, 171–199.
82 Y. Wu, G.-P. Yang, X. Zhou, J. Li, Y. Ning and Y.-Y. Wang, *Dalton Trans.*, 2015, **44**, 10385–10391.
83 R. Feng, F. L. Jiang, L. Chen, C. F. Yan, M. Y. Wu and M. C. Hong, *Chem. Commun.*, 2009, 5296–5298.
84 J. C. Rendón-Balboa, L. Villanueva-Sánchez, L. D. Rosales-Vázquez, J. Valdes-García, A. R. Vilchis-Nestor, D. Martínez-Otero, S. Martínez-Vargas and A. Dorazco-González, *Inorg. Chim. Acta*, 2018, **483**, 235–240.
85 G. K. Sidhu, S. Singh, V. Kumar, D. S. Dhanjal, S. Datta and J. Singh, *Crit. Rev. Environ. Sci. Technol.*, 2019, **49**, 1135–1187.
86 X. Xu, Y. Guo, X. Wang, W. Li, P. Qi, Z. Wang, X. Wang, S. Gunasekaran and Q. Wang, *Sens. Actuators, B*, 2018, **260**, 339–345.
87 I. J. Bazany-Rodríguez, D. Martínez-Otero, J. Barroso-Flores, A. K. Yatsimirsky and A. Dorazco-González, *Sens. Actuators, B*, 2015, **221**, 1348–1355.
88 H. Sun, Y. Y. Zhang, S. H. Si, D. R. Zhu and Y. S. Fung, *Sens. Actuators, B*, 2005, **108**, 925–932.
89 Y. Liu, K. Ai, X. Cheng, L. Huo and L. Lu, *Adv. Funct. Mater.*, 2010, **20**, 951–956.
90 M. Jaishankar, T. Tseten, N. Anbalagan, B. B. Mathew and K. N. Beeregowda, *Interdiscip. Toxicol.*, 2014, **7**, 60–72.
91 J. Ma and P. K. Dasgupta, *Anal. Chim. Acta*, 2010, **673**, 117–125.
92 L. Yang, L. Cao, X. Li, C. Qin, L. Zhao, K. Z. Shao and Z. M. Su, *Dalton Trans.*, 2017, **46**, 7567–7576.
93 Y. Y. Jia, Y. H. Zhang, J. Xu, R. Feng, M. S. Zhang and X. H. Bu, *Chem. Commun.*, 2015, **51**, 17439–17442.
94 World Health Organization, *Guidelines for drinking-water quality: fourth edition incorporating the first addendum*, Switzerland, 4th edn, 2017.
95 Codex Alimentarius, Pesticides | CODEXALIMENTARIUS FAO-WHO, http://www.fao.org/fao-who-codexalimentarius/thematic-areas/pesticides/en/#c452840, (accessed 19 February 2021).
96 C. S. Wang, Q. Huang, X. Wang, Y. T. Zhang, D. S. Ma, Y. H. Yu and J. S. Gao, *RSC Adv.*, 2019, **9**, 42272–42283.
97 D. Feng, J. Tang, J. Yang, X. Ma, C. Fan and X. Wang, *J. Mol. Struct.*, 2020, **1221**, 128841.

98 L. Fan, F. Wang, D. Zhao, X. Sun, H. Chen, H. Wang and X. Zhang, *Spectrochim. Acta, Part A*, 2020, **239**, 118467.
99 L. Fan, F. Wang, D. Zhao, Y. Peng, Y. Deng, Y. Luo and X. Zhang, *Appl. Organomet. Chem.*, 2020, **34**, 1–10.
100 C. L. Tao, B. Chen, X. G. Liu, L. J. Zhou, X. L. Zhu, J. Cao, Z. G. Gu, Z. Zhao, L. Shen and B. Z. Tang, *Chem. Commun.*, 2017, **53**, 9975–9978.
101 N. Xu, Q. Zhang and G. Zhang, *Dalton Trans.*, 2019, **48**, 2683–2691.
102 L. Yang, Y. L. Liu, C. G. Liu, F. Ye and Y. Fu, *J. Hazard. Mater.*, 2020, **381**, 120966.
103 J. Valdes-García, L. D. Rosales-Vazquez, I. J. Bazany-Rodríguez and A. Dorazco-González, *Chem. – Asian J.*, 2020, **15**, 2925–2938.